Article

Neuron

Transsynaptic Mapping of Second-Order Taste Neurons in Flies by *trans*-Tango

Highlights

- A genetic approach for transsynaptic tracing and manipulation of neural circuits
- Genetic access to neurons based on their connectivity
- Glomerulus-specific patterns of second-order neurons in the fly olfactory system
- Identifying second-order gustatory neurons and their target areas in the fly brain

Authors

Mustafa Talay, Ethan B. Richman, Nathaniel J. Snell, ..., Mark Johnson, John R. Szymanski, Gilad Barnea

Correspondence

gilad_barnea@brown.edu

In Brief

Talay and Richman et al. develop a genetic method for transsynaptic labeling of neural circuits in *Drosophila*. They validate it in the olfactory system and implement it in the gustatory system to reveal second-order projections of sweet tastant-responsive neurons.

Talay et al., 2017, Neuron *96*, 783–795
November 15, 2017
https://doi.org/10.1016/j.neuron.2017.10.011

CellPress

Neuron
Article

Transsynaptic Mapping of Second-Order Taste Neurons in Flies by *trans*-Tango

Mustafa Talay,[1,2] Ethan B. Richman,[1,2,3] Nathaniel J. Snell,[1] Griffin G. Hartmann,[1] John D. Fisher,[1] Altar Sorkaç,[1] Juan F. Santoyo,[1] Cambria Chou-Freed,[1] Nived Nair,[1] Mark Johnson,[1,4] John R. Szymanski,[1,5] and Gilad Barnea[1,6,*]
[1]Department of Neuroscience, Division of Biology and Medicine, Brown University, Providence, RI 02912, USA
[2]These authors contributed equally
[3]Present address: Neurosciences Graduate Program, Stanford University, Stanford, CA 94305, USA
[4]Present address: Beth Israel Deaconess Medical Center, Harvard Medical School, Boston, MA 02215, USA
[5]Present address: The Integrated Program in Cellular, Molecular and Biomedical Studies, Columbia University, New York, NY 10027, USA
[6]Lead Contact
*Correspondence: gilad_barnea@brown.edu
https://doi.org/10.1016/j.neuron.2017.10.011

SUMMARY

Mapping neural circuits across defined synapses is essential for understanding brain function. Here we describe *trans*-Tango, a technique for anterograde transsynaptic circuit tracing and manipulation. At the core of *trans*-Tango is a synthetic signaling pathway that is introduced into all neurons in the animal. This pathway converts receptor activation at the cell surface into reporter expression through site-specific proteolysis. Specific labeling is achieved by presenting a tethered ligand at the synapses of genetically defined neurons, thereby activating the pathway in their postsynaptic partners and providing genetic access to these neurons. We first validated *trans*-Tango in the *Drosophila* olfactory system and then implemented it in the gustatory system, where projections beyond the first-order receptor neurons are not fully characterized. We identified putative second-order neurons within the sweet circuit that include projection neurons targeting known neuromodulation centers in the brain. These experiments establish *trans*-Tango as a flexible platform for transsynaptic circuit analysis.

INTRODUCTION

Neurons are the basic structural and functional units of the nervous system (Ramón y Cajal, 1888; Sherrington, 1906). Individual neurons connect to one another via synapses to form neural circuits (De Robertis and Bennett, 1955), and the concerted activities of neurons within circuits underlie all brain functions, including perception, cognition, and generation of behavior. Our limited ability to specifically map synaptically connected neurons within circuits, or to selectively manipulate their functions, therefore, poses a major obstacle to understanding the workings of the brain. Neuroimaging techniques, such as magnetic resonance imaging, lack the resolution and precision needed to reveal synaptic connectivity, while most molecular genetic techniques are limited to the confines of the neurons for which markers exist. Other methods for circuit mapping, such as paired recording and optogenetic-assisted circuit mapping, are labor intensive and low throughput. Serial electron microscopy is the gold standard for identifying synaptic connections within a circuit, but practical considerations limit the utility of this technique to analyzing small volumes of postmortem tissue. Further, this approach is not suitable for comprehensive analysis of variability among individuals (Briggman and Bock, 2012).

The use of genetically introduced tracers, such as plant lectins and bacterial toxins, has been invaluable toward understanding neuronal connectivity (Huh et al., 2010). However, the utility of these tracers is limited by the lack of synaptic specificity and directionality. These tracers are further limited by their spread beyond one neuron and by the resulting dilution of the signal. The most commonly used transsynaptic tracing techniques in vertebrates rely on replication-deficient neurotropic viruses that are restricted to genetically defined neurons within a circuit (Callaway and Luo, 2015). While most neurotropic viruses transport only in the retrograde direction, some anterograde viral tracers have been developed (Lo and Anderson, 2011; Zingg et al., 2017). Two major limitations in the use of neurotropic viruses as tracers are the low efficiency of transsynaptic transport and the variability between experiments in the infected neuronal populations (Callaway and Luo, 2015). Another significant problem with some viral tracers is their toxicity to the infected neurons that may lead to cell death and consequent infection of irrelevant bystander neurons (Callaway and Luo, 2015). In spite of these limitations, rabies has been useful for retrograde tracing, but it is restricted to certain model organisms. By contrast, the utility of the anterograde viral tracers has been very limited.

Several techniques use versions of fluorescent proteins to label synaptic connections or to trace circuits. Transsynaptic complementation of a split version of green fluorescent protein (GFP) is used in GRASP (GFP reconstitution across synaptic partners) to mark synapses (Feinberg et al., 2008; Gordon and Scott, 2009). Each of the two complementary pieces of GFP is expressed by genetically defined neuronal populations, and functional GFP is reconstituted when both pieces are in close proximity. Modified versions of GRASP have been developed

to enhance its synaptic specificity by fusing at least one of the pieces of GFP to a synaptic protein (Fan et al., 2013; Macpherson et al., 2015). Nonetheless, these methods only label synapses rather than whole cells, and it is therefore difficult to relate the GRASP signal to particular neurons. Further, none of the versions of GRASP can be used for tracing the projections of postsynaptic neurons. Another method for circuit tracing uses photoactivatable GFP, which is genetically encoded and locally photoconverted to its high-fluorescence form to enable labeling of specific neural processes (Clowney et al., 2015; Datta et al., 2008; Patterson and Lippincott-Schwartz, 2002; Ruta et al., 2010). This approach achieves higher spatial specificity than that afforded by genetic markers, but is invasive, can label fibers-of-passage, and does not report connectivity. Finally, a major limitation of all of these tracing techniques is that they do not provide stable genetic access to the postsynaptic partners, and therefore they cannot be used to manipulate the function of the circuit.

Tango-Trace is a technique that was developed to trace projections in the fly visual system (Jagadish et al., 2014). It is based on Tango, an *in vitro* assay for recording the activation of receptors by their ligands (Barnea et al., 2008). In Tango, a synthetic signaling pathway consisting of two fusion proteins converts the activation of a cell-surface receptor into reporter expression via site-specific proteolysis (Barnea et al., 2008). Tango-Trace employed a configuration of Tango for detecting histamine, the excitatory neurotransmitter released from photoreceptors in the fly retina upon activation (Jagadish et al., 2014). The utility of Tango-Trace has been rather limited because outside the retina histamine mostly serves as a neuromodulator rather than a neurotransmitter (Hong et al., 2006; Nässel, 1999). Further, diffusion of histamine away from the synapse and consequent labeling of non-synaptic neurons is a potential problem with Tango-Trace.

Here we describe *trans*-Tango, a method for anterograde transsynaptic tracing. While *trans*-Tango is also based on the Tango assay, its design is fundamentally different than Tango-Trace in order to generate a general and flexible transsynaptic labeling system. *trans*-Tango employs an exogenous ligand-receptor pair for circuit labeling, so in principle it can be applied to any neural circuit regardless of the neurotransmitter that it uses and without making any assumptions about the nature of the connection. To present the ligand, we introduce a third fusion protein in which the ligand is tethered to a synaptic protein via an extracellular spacer. This configuration directs the ligand to the synapse and prevents it from diffusing away. In *trans*-Tango, the Tango signaling pathway is introduced into all neurons in the animal. Specific labeling is achieved by presenting the tethered ligand at the synapses of genetically defined neurons, thereby activating the signaling pathway only in their postsynaptic partners. We designed *trans*-Tango in a modular fashion to allow easy integration with other genetic tools for circuit dissection and manipulation. We first validated *trans*-Tango in the olfactory system of the fruit fly *Drosophila melanogaster*, where our experiments recapitulated known connections but also revealed new ones. We then used *trans*-Tango to identify hitherto unknown second-order neurons in the *Drosophila* gustatory system. Our anatomical tracing experiments revealed that second-order gustatory neurons target brain areas known to be involved in neuromodulation and in controlling feeding behaviors, providing a possible pathway for integrating gustatory signals and the regulation of feeding.

RESULTS

Transsynaptic Labeling by *trans*-Tango

trans-Tango is a transsynaptic labeling system that is based on Tango, a cellular assay for recording the activation of specific receptors by their ligands (Barnea et al., 2008). In Tango, a synthetic signaling pathway is activated in response to ligand binding to its receptor through a specific proteolytic event that releases a membrane-tethered transcription factor, allowing it to translocate into the nucleus and induce expression of a reporter (Barnea et al., 2008). To attain anterograde labeling by *trans*-Tango, we expressed the core components of the signaling pathway panneuronally and presented the ligand that activates the pathway at presynaptic sites in a neural circuit. Contact between the ligand and its receptor at synaptic sites drives expression of a reporter in postsynaptic neurons. The ligand and its receptor are exogenous to the animal in order to prevent spurious signal. To establish *trans*-Tango in *Drosophila*, we used human glucagon and its receptor as the ligand-receptor pair.

The signaling pathway driving postsynaptic reporter expression consists of three components (Figure 1A). The first is a fusion protein comprising the glucagon receptor, a G protein-coupled receptor, bound at its cytoplasmic tail to the transcriptional activator QF (Potter et al., 2010) via a linker containing the cleavage site for the highly specific N1a protease from the tobacco etch virus (TEV) (Barnea et al., 2008). The second component, hArr::TEV, is a fusion between TEV and human β-arrestin2, a protein that is specifically recruited to activated G protein-coupled receptors (Barnea et al., 2008). Panneuronal promoters drive expression of these two fusion proteins in all neurons. The third component in the pathway is a reporter, such as mtdTomato, under transcriptional control of QF. In this manner, all neurons in the fly are endowed with the capacity to express the reporter upon activation of the signaling pathway. The pathway is activated only in neurons that are postsynaptic to those that express a membrane-tethered form of glucagon at their presynaptic terminals (see below). In the absence of ligand at a given synapse, QF is sequestered to the membrane, and the reporter is not expressed (Figure 1A, top). By contrast, at synapses where the ligand is expressed, transsynaptic activation of the receptor leads to recruitment of hArr::TEV. Upon TEV cleavage in its target site, QF is released from the membrane, allowing it to enter the nucleus and induce reporter expression (Figure 1A, bottom). The inherent signal amplification by the signaling pathway renders *trans*-Tango very sensitive, and since the components of the signaling pathway are extrinsic to the cell, background noise can be kept low. Thus, *trans*-Tango should label circuits with high signal-to-noise ratios.

In order to localize glucagon to the synapse and present it to postsynaptic receptors, we generated another fusion protein consisting of the cytosolic and transmembrane domains of the synaptic protein *Drosophila* Neurexin1, the large extracellular domain of the human cell-adhesion molecule ICAM1, a flexible linker including a myc-tag (Fortin et al., 2009), and a mutated

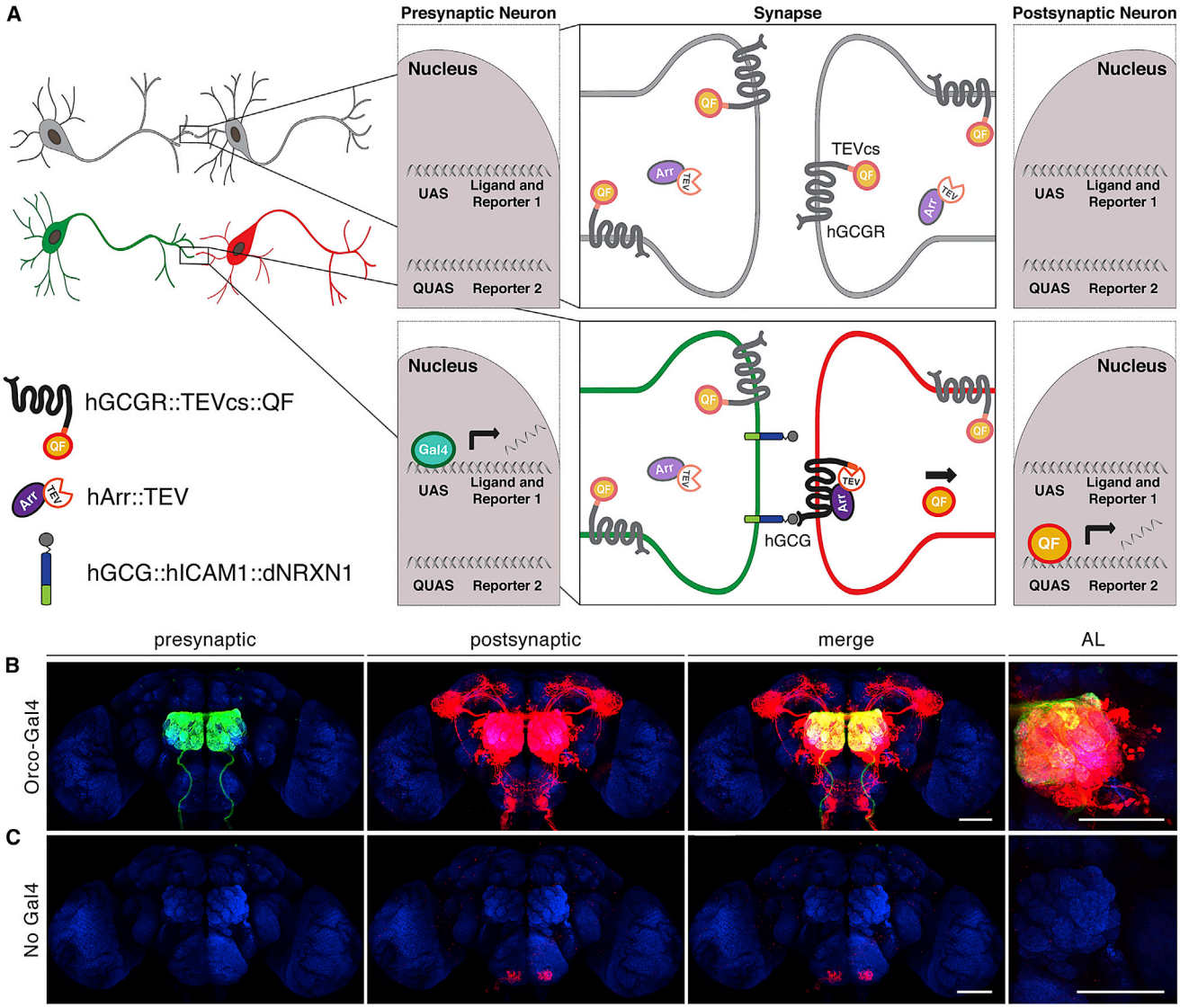

Figure 1. Design and Implementation of *trans*-Tango in the Fly Olfactory System

(A) Schematic design of *trans*-Tango. The general design of *trans*-Tango is based on the Tango assay in a configuration for human glucagon. In *trans*-Tango, the components of the Tango signaling pathway (hGCGR::TEVcs::QF and hArr::TEV) are expressed in all neurons, rendering them competent for QF-dependent expression of Reporter 2 (red). The signaling pathway is transsynaptically activated by a membrane-tethered form of glucagon that is fused to the transmembrane and cytoplasmic domains of the *Drosophila* synaptic protein Neurexin1 via a spacer consisting of the extracellular domain of the human cell adhesion molecule ICAM1 and a flexible linker (hGCG::hICAM1::dNRXN1). Expression of the ligand fusion and Reporter 1 (green, to mark the presynaptic neuron) are Gal4 dependent. In the absence of ligand, the transcription factor QF stays tethered to the receptor; hence, there is no expression of Reporter 2 (top). Ligand expression in the presynaptic neuron activates the signaling pathway in the postsynaptic neuron, releasing QF to translocate into the nucleus and initiate Reporter 2 expression from QUAS (bottom).

(B) In flies bearing the *trans*-Tango components, driving ligand and myrGFP expression in the majority of ORNs targeting the AL by *Orco*-Gal4 (green) results in mtdTomato expression in postsynaptic LNs and PNs (red).

(C) No signal is observed in flies bearing the *trans*-Tango components without a Gal4 driver, except for some background noise in the ventral SEZ. (B and C) The right panels are zoomed-in on the AL. Max-projection pictures of whole-mount brains are shown. Blue, neuropil counterstain. Scale bars, 50 μm. See also Figure S1 and Movie S1.

version of the glucagon peptide with high potency for glucagon receptor activation (Krstenansky et al., 1986) (Figures 1A and S1A). The resulting *trans*-Tango ligand, which is sized to extend across the average length of a synapse, is enriched in axons (Figure S1B) and targeted to axon termini (Figure S1C). By contrast, another version of the tethered ligand in which glucagon is fused to CD4, a cell surface protein that lacks synaptic localization, resulted in ligand expression throughout the neuron (data not shown). To enhance the flexibility of *trans*-Tango, the expression of the ligand fusion protein is controlled

by the Gal4-UAS binary system (Brand and Perrimon, 1993), the most commonly used tool for genetic access in flies.

To introduce the *trans*-Tango components into the fly, we generated a transgenic line bearing all three fusion proteins as a single allele (*trans*-Tango): (1) the receptor fusion, (2) hArr::TEV, and (3) the ligand fusion (Figure S1A). We did not detect any effect of panneuronal expression of the *trans*-Tango components on normal lifespan, development, brain morphology, or motor behavior (data not shown). We generated a second transgenic line bearing a reporter allele containing a membrane-associated form of GFP under control of Gal4 (*UAS*-myrGFP) to mark presynaptic neurons, and a membrane-associated form of tdTomato under control of QF (*QUAS*-mtdTomato) to mark postsynaptic neurons (Figures 1A and S1A). In this manner, any circuit for which a presynaptic Gal4 driver is available can in principle be traced by *trans*-Tango. To achieve this, flies bearing the *trans*-Tango and reporter alleles are crossed to flies bearing the appropriate Gal4 driver, and offspring carrying all three alleles are analyzed.

Validating *trans*-Tango in the Olfactory System

We sought to validate *trans*-Tango in the context of the well-characterized olfactory system. *Drosophila* olfactory receptor neurons (ORNs) express specific receptors and detect volatile odors. ORNs residing in the antenna and maxillary palp project to the antennal lobe (AL), where ORNs expressing a given receptor converge on the same neuropil structures called glomeruli. Axons from ORNs synapse with local interneurons (LNs) and projection neurons (PNs) (Vosshall and Stocker, 2007). LNs project locally to other glomeruli within the AL, while PNs project from the AL to the mushroom body (MB) calyx and the lateral horn (LH) mainly via the medial, mediolateral, and lateral antennal lobe tracts (mALT, mlALT, and lALT, respectively) (Ito et al., 2014).

We first used *Orco*-Gal4, which is expressed in the majority of ORNs (Vosshall and Stocker, 2007), to drive expression of the *trans*-Tango ligand and myrGFP. In flies bearing the *Orco*-Gal4 driver and the *trans*-Tango components, we observed the typical innervation of the AL by GFP-expressing ORNs and robust mtdTomato labeling in LNs as well as in PNs that target the MB calyx and LH (Figure 1B and Movie S1). In addition, we observed projections descending to the subesophageal zone (SEZ), the first processing center for gustatory information in the brain (Ito et al., 2014; Wang et al., 2004). We observed a total of 152 ± 6 (mean ± SD) and 182 ± 17 postsynaptic neurons per hemisphere in females and males, respectively (n = 10 ALs per group). By contrast, no signal, except two spots in the ventral SEZ, was detected in the brains of control flies bearing the *trans*-Tango components and no Gal4 driver, which is necessary for *trans*-Tango ligand expression (Figure 1C). The background noise in the ventral SEZ might be due to sporadic leaky expression known to occur in the attP40 genomic locus where we integrated the *trans*-Tango allele (Pfeiffer et al., 2010). These results demonstrate the tight regulation of ligand-dependent QF release and the consequent high signal-to-noise ratio of *trans*-Tango.

Specificity of *trans*-Tango

To examine the specificity of *trans*-Tango, we expressed the ligand in individual ORN classes. We started with one of the most studied olfactory circuits in flies, Or67d-expressing ORNs that target the DA1 glomeruli and mediate sexual behaviors (Datta et al., 2008; Jefferis et al., 2007; Kurtovic et al., 2007; Ruta et al., 2010). Expression of the *trans*-Tango ligand in Or67d+ ORNs resulted in an extremely dense signal in LNs innervating many glomeruli including DA1 and also led to specific labeling of PNs targeting the MB calyx and LH (Figure 2A). Additionally, we found bilateral descending projections from the AL to the SEZ (Figure 2A, arrows), as we noticed with the broadly expressed *Orco*-Gal4 (Figure 1B). We observed a total of 61 ± 5 and 81 ± 4 postsynaptic neurons per hemisphere in females and males, respectively (n = 10 ALs per group). In subsequent experiments, we expressed the ligand in Or42b-expressing ORNs that are important for detecting certain food odors (Root et al., 2011; Semmelhack and Wang, 2009). We observed dense *trans*-Tango-dependent signal in LNs innervating many glomeruli, including the cognate DM1 glomerulus, as well as signal in a distinct set of PNs projecting to the MB calyx and LH (Figure 2B). We observed a total of 86 ± 7 and 92 ± 5 postsynaptic neurons per hemisphere in females and males, respectively (n = 10 ALs per group). It is noteworthy that the reporter in *trans*-Tango is integrated in the X chromosome, so due to dosage compensation, the signal in males is higher than in heterozygous females. Thus, while the cell number differences between males and females could reflect sexual dimorphism, they could also result from the difference in reporter levels. These results, together with *trans*-Tango labeling of other ORN classes (Figure S2), confirm the high degree of interconnectivity among glomeruli suggested by earlier studies (Chou et al., 2010; Seki et al., 2010).

While the general patterns of postsynaptic signal were similar for the various ORN populations, careful examination revealed notable differences. Namely, with ligand expressed in Or42b+ ORNs, we did not observe the neurons descending from the AL to the SEZ (Figures 2A and 2B, arrows). In addition, the targeting patterns of the two PN populations within the LH were distinct, with projections from DA1 terminating in the ventral LH and those from DM1 terminating more dorsally (Figures 2A and 2B). These projection patterns are in agreement with the literature (Jefferis et al., 2007; Strutz et al., 2014). Finally, while we observed postsynaptic signal from both DA1 and DM1 throughout the AL, the signal distribution was not homogeneous and was different between the two. The postsynaptic signal from the DA1 glomerulus was sparser in the medial aspect of the AL, an area that includes DM1 among other glomeruli. By contrast, the postsynaptic signal from DM1 was sparser in the lateral aspect of the AL, an area that includes DA1 (Figures 2A and 2B). The different postsynaptic signal patterns produced by driving *trans*-Tango ligand expression in different classes of ORNs, and the agreement with known projection patterns, suggest that *trans*-Tango reveals specific postsynaptic partners.

In our attempts to optimize *trans*-Tango, we examined the effects of temperature and age on the *trans*-Tango signal. We found an inverse correlation between the *trans*-Tango signal and temperature over the range of 15°C–25°C, with the best signal-to-noise ratio observed at 18°C (Figure S3), while Gal4-dependent signal increased with temperature in this range as expected (Wilder and Perrimon, 1995). In flies raised at 18°C, *trans*-Tango output labeling for three different populations of ORNs gradually increased with age, starting to saturate at

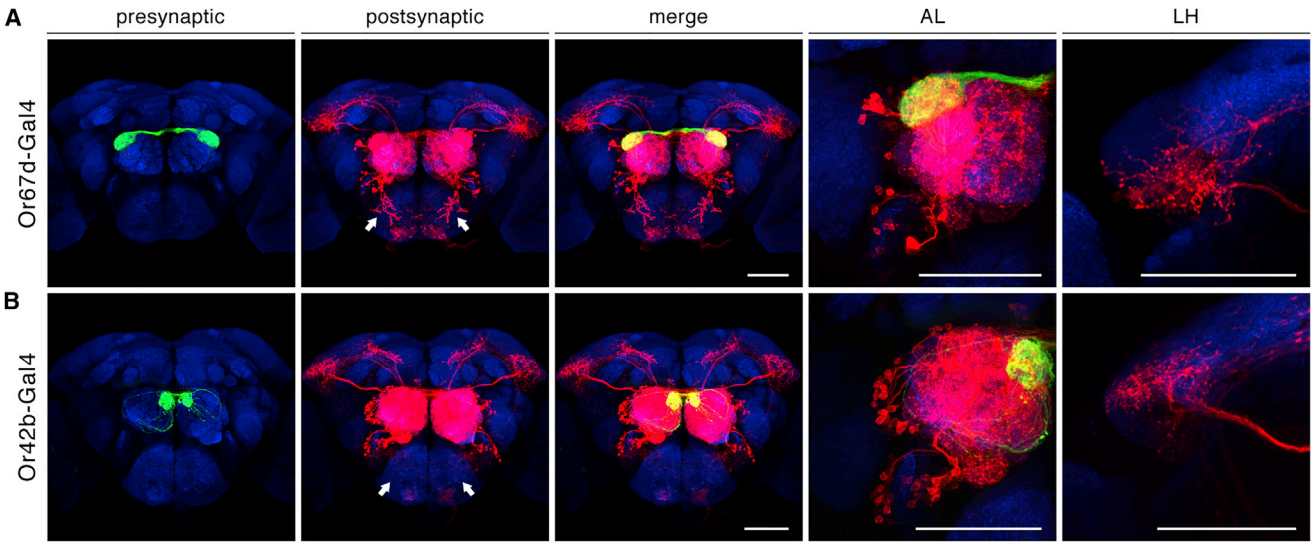

Figure 2. Specificity of *trans*-Tango

(A and B) Expression of the *trans*-Tango ligand in Or67d+ (A) and in Or42b+ (B) ORNs (green) reveals distinct projection patterns (red). Note the postsynaptic signal of Or67d+ ORNs that descends to the SEZ (arrows) and is absent when the ligand is expressed in Or42b+ ORNs. The right panels are zoomed-in on the AL and LH. Max-projection pictures of whole-mount brains are shown. Blue, neuropil counterstain. Scale bars, 50 μm. See also Figures S2–S10.

approximately 2 weeks post-eclosion (Figures S4–S6). We therefore maintained the flies for all of our experiments at 18°C and analyzed them at least 2 weeks post-eclosion.

It is noteworthy that we observed linkage between the strength of the Gal4 line used to drive the ligand and the intensity of the *trans*-Tango output signal (data not shown). This was apparent even when comparing different genomic integrations of the same Gal4 drivers (data not shown). Hence, the optimal age for analysis should be established empirically for each Gal4 driver of interest. Finally, we wished to examine individual variability in projection patterns among flies of the same genotype. We compared the postsynaptic projections from the DA1 and DM1 glomeruli in age-matched flies and observed consistent projection patterns within groups (Figures S7–S10). These results showcase the strength of *trans*-Tango as a genetic system to generate reproducible transsynaptic labeling results between individuals.

Sparse Labeling of Postsynaptic Neurons with *trans*-Tango

The widespread mtdTomato labeling in the AL impeded our ability to determine whether the labeled PNs were indeed receiving input from the proper glomerulus. We therefore pursued mosaic-labeling strategies to isolate individual postsynaptic neurons. We used *trans*-Tango in conjunction with MARCM (Lee and Luo, 1999; Potter et al., 2010) to label postsynaptic neurons singly or in small groups. Suppression of the QF-dependent postsynaptic signal was achieved with pancellular expression of QS (Potter et al., 2010) and relieved in stochastic subsets of cells by heat shock. Importantly, MARCM analysis of postsynaptic neurons that were labeled via ligand expression in Or67d+ ORNs revealed PNs or LNs with dendrites arborizing within the DA1 glomerulus (Figure 3A, data not shown). Likewise, equivalent experiments with Or42b+ ORNs revealed neurons contacting the cognate DM1 glomerulus (data not shown). With both populations, obtaining single cell clones with MARCM was rare. Notably, when the ligand was expressed in Or67d+ ORNs, we obtained brains in which a single neuron projecting between the AL and SEZ was observed. This neuron innervates the DA1 glomerulus along with a number of other glomeruli (Figure 3A).

To further characterize the putative postsynaptic neurons of Or67d+ ORNs, we implemented an intersectional Flp-out strategy for *trans*-Tango, in which QF-dependent reporter expression required the FLP recombinase (Gordon and Scott, 2009; Potter et al., 2010). By combining this intersectional reporter with initiation of *trans*-Tango labeling from Or67d+ ORNs, we were able to restrict labeling to Fru+ or GH146+ neurons (Figures 3B and 3C, respectively). We observed 10 ± 2 Fru+ PN cell bodies per hemisphere in females and 6 ± 1 in males (n = 12 ALs per group), and 23 ± 2 GH146+ PNs in females and 23 ± 3 in males (n = 22 ALs for females and 20 for males). A similar strategy driving the system from Orco+ ORNs revealed 93 ± 7 PNs in females and 98 ± 6 in males (n = 12 ALs per group). Interestingly, these intersectional experiments with ligand expressed in Or67d+ ORNs revealed that the neuron projecting from the AL to the SEZ is Fru+ (Figure 3B, arrows), suggesting that this neuron might play a role in connecting pheromone responses and gustation.

Sensitivity and Versatility of *trans*-Tango

The adult olfactory circuits are characterized by a convergence of many ORNs onto the output neurons in the AL. This architecture results in concentration of the *trans*-Tango ligand from many neurons onto the postsynaptic neurons. Many other circuits are less convergent, and may not yield such concentration of ligand onto postsynaptic receptors. The ability to label postsynaptic

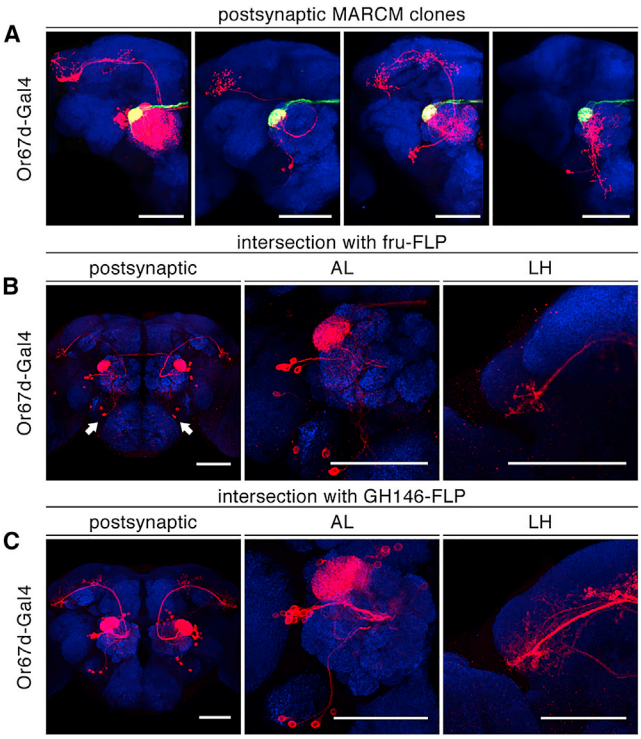

Figure 3. Sparse Labeling of Postsynaptic Neurons with *trans*-Tango

(A) Sparse labeling of postsynaptic neurons through combining *trans*-Tango with MARCM. Clones of different postsynaptic neurons (red) receiving input from the DA1 glomerulus (green) are shown for four different individuals.

(B and C) Sparse labeling of genetically defined postsynaptic neurons via FLP recombination. Combining *trans*-Tango with FLP recombination enables intersectional labeling of FLP+ postsynaptic neurons. Postsynaptic signal is expressed by removing the stop cassette in the conditional reporter (red) using *fru*-FLP (B) and *GH146*-FLP (C). Arrows in (B) point to the neurons descending to the SEZ. The right panels are zoomed-in on the AL and LH. (A–C) Max-projection pictures of whole-mount brains are shown. Blue, neuropil counterstain. Scale bars, 50 μm.

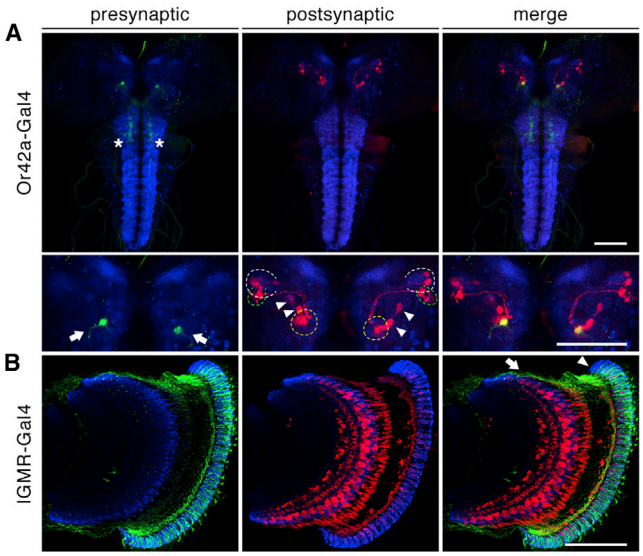

Figure 4. Sensitivity of *trans*-Tango

(A) Expression of the *trans*-Tango ligand in Or42a+ ORNs in the larva (a single ORN per side, green, arrows) leads to labeling of PNs (red, arrowheads). *trans*-Tango is combined with intersectional genetics to restrict the postsynaptic signal to *GH146*-FLP+ PNs, as the leakiness of the UAS promoter in the larval ventral nerve cord (green, asterisks) results in background noise (data not shown). In the lower zoomed-in panels of the larval central brain, the AL, MB calyx, and LH are indicated by dashed lines in yellow, white, and green, respectively. Max-projection pictures of a whole-mount brain are shown.

(B) Implementation of *trans*-Tango in the visual system. Expression of the ligand in lGMR+ photoreceptor cells (green) induces postsynaptic signal (red) in the lamina (arrowhead) and medulla (arrow). A single optical section through the adult optic lobe is shown. (A and B) Blue, neuropil counterstain. Scale bars, 50 μm.

partners of a single presynaptic neuron is essential for the precise characterization of circuits. We therefore sought to determine whether *trans*-Tango could illuminate output neurons that receive input from single ligand-expressing neurons. We chose to examine this in the larval olfactory system, in which distinct olfactory receptor genes are expressed by single ORNs (Fishilevich et al., 2005). However, when we examined larvae carrying the *trans-Tango* allele, we observed mtdTomato expression in the ventral nerve cords (VNCs) of both the experimental and control larvae (data not shown). Careful examination of the VNCs revealed GFP expression, albeit faintly (Figure 4A, asterisk), suggesting that our UAS promoters might be leaky in the larval VNC, leading to Gal4-independent expression of ligand that induces *trans*-Tango-mediated mtdTomato expression. This background labeling in the larval VNC is not observed in flies lacking the *UAS*-glucagon component (data not shown). We therefore decided to use an intersectional approach where the signal is limited to the olfactory system through the use of *GH146*-FLP together with a conditional suppressor (*tubP-FRT-QS-FRT*) that we have generated. In larvae bearing these alleles together with *trans*-Tango driven from Or42a+ ORNs, we observed 3 ± 1 GH146+ PNs per hemisphere (n = 22 ALs) (Figure 4A). These results in the larval olfactory system suggest that *trans*-Tango is sensitive enough to label the outputs of single neurons. We note that because various circuits exhibit a range of densities of synapses, the sensitivity of *trans*-Tango may lessen in circuits with sparser synaptic contacts.

To further determine whether *trans*-Tango could be used in circuits with other architectures, we investigated the peripheral visual system, where the architecture is mostly columnar (Morante and Desplan, 2008). We expressed the *trans*-Tango ligand in lGMR+ photoreceptor cells and observed widespread postsynaptic labeling in the lamina and medulla (Figure 4B). The implementation of *trans*-Tango to label visual circuits illustrates the flexibility of the system and its utility for studying circuits with diverse architectures and properties.

Identifying Second-Order Taste Neurons and Their Projections in the Brain

We next turned our attention to the gustatory system, where relatively little is known about the postsynaptic partners of gustatory receptor neurons (GRNs) (Harris et al., 2015; Kain and Dahanukar, 2015; Kim et al., 2017; Miyazaki et al., 2015; Yapici et al., 2016). GRNs express gustatory receptors (GRs) that detect

non-volatile chemicals and are dispersed in various parts of the body, including the proboscis (labellum and pharynx), tarsal segments of the legs, wing margins, abdomen, intestine, and female genitalia (Clyne et al., 2000; Dunipace et al., 2001; Scott et al., 2001; Vosshall and Stocker, 2007). Each one of these peripheral gustatory organs is thought to contribute distinctly to the overall gustatory response of the fly to tastants (Vosshall and Stocker, 2007). Distinct populations of GRNs respond to sweet and bitter tastants (Harris et al., 2015). Like mammals, flies respond to sweet and bitter tastants with different behavioral outputs: sweet molecules are attractive and elicit acceptance, while bitter compounds are aversive and lead to rejection (Vosshall and Stocker, 2007). The clear linkage between stimulus quality and behavioral response suggests differential representation of taste categories in the brain. Indeed, the projections of GRNs responding to sweet and bitter tastants segregate within the SEZ (Wang et al., 2004). However, little is known about the nature of subsequent projections from the SEZ, or about how gustatory information is processed further to elicit the appropriate behavioral outputs.

Seeking to identify second-order neurons in the gustatory system, we initiated expression of the *trans*-Tango ligand in Gr64f+ sweet GRNs. Expression of the *trans*-Tango ligand in Gr64f+ GRNs revealed extensive postsynaptic signal in the CNS (Figures 5A and 5B, Movie S2). Gr64f+ GRNs are present in each leg and either terminate in the thoracic ganglia or project directly to the posterior SEZ with collaterals in the thoracic ganglia (Figure 5A) (Kwon et al., 2014; Thoma et al., 2016). Gr64f+ GRNs also innervate the abdominal ganglion (Movie S2). Expression of the Tango ligand in Gr64f+ GRNs induced postsynaptic mtdTomato signal in each thoracic neuromere and in the abdominal ganglion in the VNC and in projections to the central brain (Figures 5A and 5B, Movie S2).

In the central brain, expression of the *trans*-Tango ligand in Gr64f+ GRNs revealed a large number of postsynaptic neurons (Figure 5B, Movie S2). The observed signal was saturated in the vicinity of the SEZ, most likely due to dense interconnectivity. It was therefore difficult to precisely discern specific connections. Most of the distinguishable cell bodies of the second-order neurons resided external to the SEZ, in the cell body rind of neighboring neuropil structures such as the antennal mechanosensory and motor center (AMMC). Additional groups of cell bodies were located posteroventral and anterodorsal to the SEZ, as well as dorsal to the AL. Due to the intense mtdTomato labeling in the SEZ, we were unable to distinguish cell bodies from cell processes there (Figure 5B).

In addition to the dense signal in the vicinity of the SEZ, we observed projections to distant neuropil structures. These projections appeared to follow three major tracts: (1) an axon bundle that projected along the midline toward the superior medial protocerebrum (SMP), where it arborized away from the midline; (2) an axon bundle that traveled posterior to the AL and arborized in the superior intermediate protocerebrum (SIP) and superior lateral protocerebrum (SLP); and (3) a thinner bundle that passed through the posterior ventrolateral protocerebrum and projected to the SLP and lateral protocerebrum (Figures 5B and 5D, Movie S2). Although the locations of the cell bodies varied across individuals, these projection tracts appeared to be stereotyped. These findings implicate the SMP, SIP, and SLP as target areas for second-order neurons in the gustatory circuits. Following the naming convention of second-order olfactory pathways (Ito et al., 2014), we refer to these gustatory tracts as medial, mediolateral, and lateral SEZ tracts (mSEZt, mlSEZt, and lSEZt, respectively).

In order to discern the precise connectivity of second-order gustatory neurons and overcome the dense signal, we combined *trans*-Tango with MARCM, or FLP-out, to stochastically reveal labeling in clonal subsets of neurons postsynaptic to Gr64f+ GRNs (Figure 5C). We observed many local interneurons that exhibited diverse arborizations within the SEZ (Figure 5C). These neurons mainly inhabited the outer layer of the neighboring AMMC and sent diffuse processes that mostly arborized on the ipsilateral side (Figure 5C). Neurons with similar morphology have been described (Kain and Dahanukar, 2015; Miyazaki et al., 2015; Yapici et al., 2016). We also observed clusters of neurons that projected to the SMP, SIP, and SLP. Our experiments revealed two distinct clusters of neurons that projected through the mSEZt: a cluster of cell bodies posteroventral to the SEZ and a cluster anterodorsal to the SEZ (Figure 5C). Neurons in the posteroventral cluster received input from the ipsilateral SEZ and projected to the ipsilateral SMP, where they branched laterally. By contrast, neurons in the anterodorsal cluster received input from both sides of the SEZ and projected to the SMP, where they branched bilaterally. We observed a single cluster of neurons that projected through mlSEZt (Figure 5C). The cell bodies of these neurons resided anterodorsal to the AL. They received input mostly from the contralateral SEZ, with a faint connection to the ipsilateral SEZ, and projected contralaterally, forming crescent-shaped terminals in the SIP/SLP. Interestingly, neurons with similar morphology were previously described as being sexually dimorphic, with females having fewer neurons and lacking input from the ipsilateral SEZ (Chiang et al., 2011; Kimura et al., 2005). Indeed, comparison between these neurons in female and male brains revealed that their morphology is different; in females the fiber connecting the cell bodies and the ipsilateral SEZ is missing (data not shown). Finally, we observed two clusters of neurons projecting through the lSEZt. The cell bodies of neurons within the first cluster resided in the cell body rind of the AMMC (Figure 5C). These neurons extended dense arborizations into the ipsilateral SEZ and more sparse arborizations into the medial aspect of the contralateral SEZ. Following the lSEZt, they projected largely to the ipsilateral SLP with minor collaterals in the lateral protocerebrum. The cell bodies of the neurons within the second cluster projecting through the lSEZt resided near the abdominal ganglion in the VNC (Figure 5C). These neurons cross the midline and ascend toward the central brain receiving input from each contralateral leg neuromere. In the central brain, they extended dense arborizations into the contralateral SEZ and some continue through the lSEZt to the contralateral SLP with minor collaterals in the lateral protocerebrum (Figure 5C). Similar long-range sweet projection neurons have been recently described (Kim et al., 2017). Interestingly, neurons with similar morphology were also described for pheromone detection

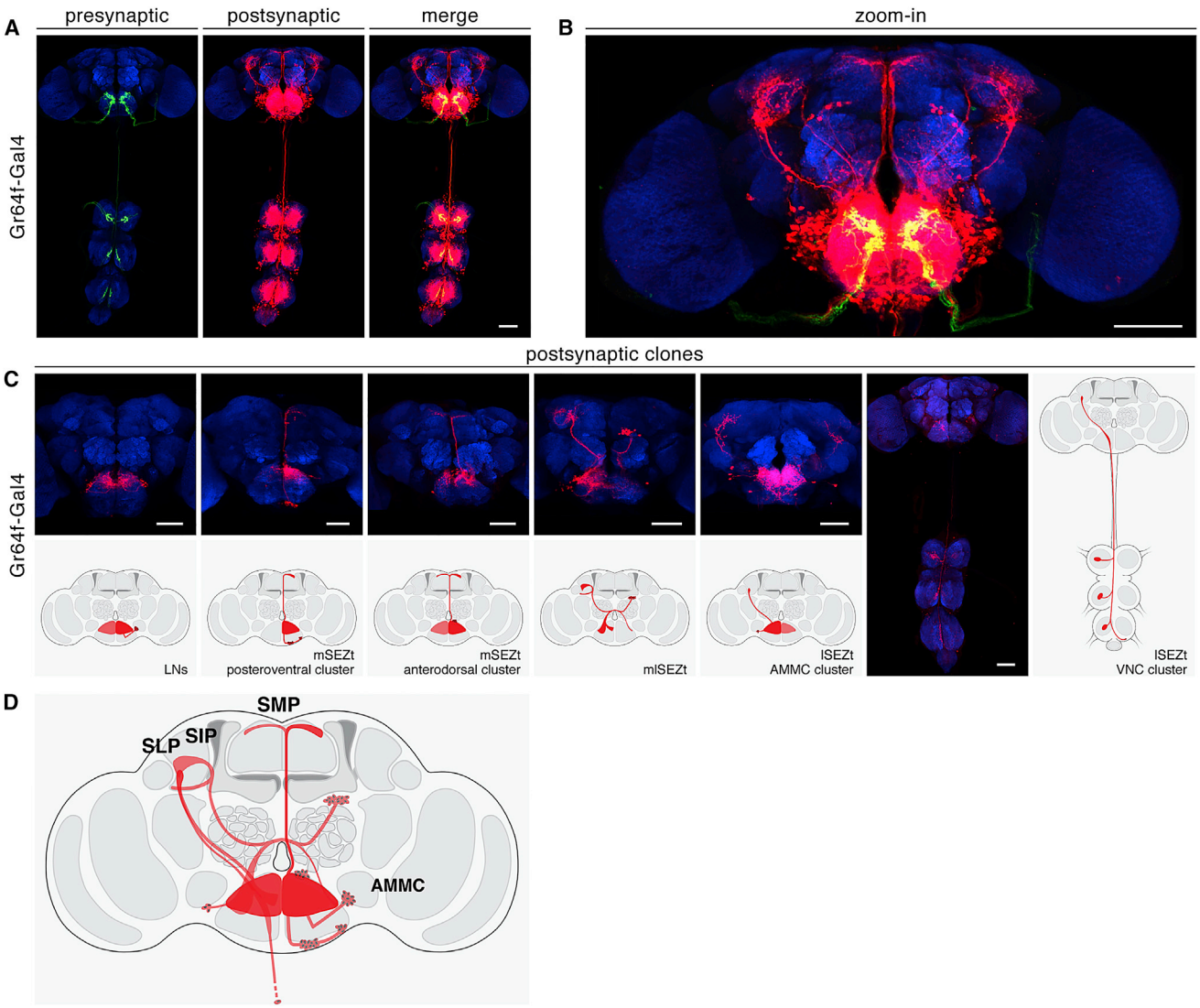

Figure 5. Second-Order Neurons of the Gustatory System Revealed by *trans*-Tango

(A) Expression of the *trans*-Tango ligand in Gr64f+ sweet sensory neurons (green) reveals second-order neurons of the gustatory system (red) targeting the VNC and the central brain.

(B) Zoomed-in picture of the central brain.

(C) Sparse labeling of second-order neurons of Gr64f+ GRNs by clonal analysis restricts the postsynaptic signal (red) to distinct neuronal clusters. Representative clones from distinct pathways are shown in each panel, and these pathways are illustrated unilaterally for simplicity.

(D) Schematic summary of a unilateral representation of the various projections shown in (B and C). See text for details. (A, B, and C) Max-projection pictures of whole-mount brains are shown. Blue, neuropil counterstain. Scale bars, 50 μm.

(Clowney et al., 2015; Yu et al., 2010). It is noteworthy that each cluster of postsynaptic neurons projected along a single tract; we never observed a neuron with parallel projections through multiple tracts (Figure 5C). While we have described here the most common projections, we also observed other projection neurons from the SEZ to the protocerebrum that did not fit in these clusters (Movie S2 and data not shown). Neurons with similar morphologies to all the classes of second-order gustatory neurons that we have identified had been described in single cell resolution (Chiang et al., 2011).

DISCUSSION

In this study, we describe *trans*-Tango, a method that we have developed for transsynaptic mapping and manipulation of neural circuits in the anterograde direction. The design of *trans*-Tango is based on the Tango assay for recording ligand-receptor interactions (Barnea et al., 2008). The Tango assay was also the basis for two earlier *in vivo* systems in *Drosophila*: TANGO-map, a method for identifying sites of neuromodulation (Inagaki et al., 2012), and Tango-Trace, which was used to functionally map projections in the visual system (Jagadish et al., 2014). Both of

these techniques used the Tango design for detecting endogenous ligands (dopamine in TANGO-map, histamine in Tango-Trace). Unlike these earlier Tango-based systems, *trans*-Tango employs exogenous ligand and receptor for circuit labeling, so in principle it can be applied to any neural circuit regardless of the neurotransmitter that it uses. Further, since in *trans*-Tango the ligand is tethered to a synaptic protein, it does not diffuse away from the synapse, a potential problem with Tango-Trace (Jagadish et al., 2014). Thus, *trans*-Tango is truly a general and flexible transsynaptic labeling technique that allows discovery of unknown synaptic partners and circuit elements without any assumptions or previous knowledge about the nature of these connections. In this manner, *trans*-Tango is a powerful tool for generating hypotheses regarding potential connectivity. Unlike other techniques for anterograde tracing, such as dye injection or the use of neurotropic viruses, *trans*-Tango is immune to signal diffusion. Further, as it can be readily combined with mosaic or intersectional approaches for sparse labeling of postsynaptic neurons, *trans*-Tango is especially suitable for tracing projections within dense neuropil.

Our experiments revealed an inverse correlation between the intensity of the postsynaptic *trans*-Tango signal and the temperature in which the flies were raised over the range of 15°C–25°C. To maximize the signal-to-noise ratio, we maintained the flies for all of our experiments at 18°C. It is noteworthy that this inverse correlation extends beyond signal intensity per neuron. Indeed, we consistently observe signal in more neurons at lower temperatures (15°C–18°C) than at 25°C. We believe that as flies are ectotherms this difference could reflect the effect of the low temperature on biological processes, such as pruning. Alternatively, this phenomenon could be directly related to features of *trans*-Tango. For example, it is conceivable that the folding of the synthetic fusion proteins in *trans*-Tango is more efficient at lower temperature, or that their turnover is slower, such that the concentrations of the various components are higher. Otherwise, perhaps the kinetics of the various interactions in *trans*-Tango (e.g., ligand-receptor interaction, recruitment of β-arrestin2 to the activated receptor, processivity of TEV, interaction between QF and QUAS, etc.) is differentially affected by temperature such that the signaling pathway is sensitized. In both cases, the overall sensitivity of the system would be much higher at lower temperatures. Consequently, even transient interactions between axons during development might result in some signal. Whatever the explanation, this phenomenon could in fact act as a knob that controls the gain of the system, and it should be considered when using it. When the goal is to reveal as many potential postsynaptic partners as possible, the flies should be raised at 15°C–18°C, but when a more stringent assessment of connectivity is desired, the flies should be raised at 25°C. This phenomenon also impacted the interpretation of the numbers of postsynaptic neurons that we observed compared to the literature, as most published data are obtained at 25°C.

Comparison of the numbers of postsynaptic neurons that we have observed with the available published numbers revealed that in some cases, our numbers corresponded with the published numbers, while in others, our numbers were higher. For example, earlier studies revealed that Or67d+ ORNs provide input onto six Fru+ PNs both in females and males (Datta et al., 2008; Ruta et al., 2010). In our experiments, driving *trans*-Tango from Or67d+ ORNs and restricting the signal to Fru+ neurons, we observed 10 ± 2 Fru+ PN cell bodies per hemisphere in females and 6 ± 1 in males, suggesting thorough labeling of postsynaptic partners by *trans*-Tango. However, we observed 23 ± 2 GH146+ PNs in females and 23 ± 3 in males. These numbers are higher than the numbers published recently: 8 ± 2 uniglomerular PNs in females and 10 ± 1 uniglomerular PNs in males (Grabe et al., 2016). This trend extends to the number of PNs associated with other glomeruli (data not shown). Similarly, when we drive *trans*-Tango from Or42a+ ORNs in larvae, we observed 3 ± 1 GH146+ PNs compared to the suggested one PN (Ramaekers et al., 2005). The higher numbers observed with *trans*-Tango could of course represent false-positive signal that might have resulted from inefficient synaptic localization of the ligand due to its overexpression, as was observed for synaptic GRASP (Chen et al., 2014). Such ligand mislocalization could have been exacerbated by the relatively late age in which we analyze the flies. In considering this discrepancy further, it is noteworthy that we chose to bias the current configuration of *trans*-Tango toward high sensitivity even at the expense of increasing the number of false positives. In this vein, we intentionally counted cells in a non-stringent manner; we counted cells even if the signal in them was faint in order to reveal any potential postsynaptic neurons. This was especially significant in the anterodorsal cluster of PNs in the olfactory system where we often saw weak signal. The difference in numbers could also be explained by the experimental approach: our numbers resulted from intersectional experiments where FLP was used, while the published numbers were generated using Gal4. As discussed earlier, temperature could be a major factor: all of our experiments were conducted at 18°C where the signal-to-noise with *trans*-Tango is optimal, but the system is more sensitive. Indeed, when the flies were raised at 25°C and PNs were counted at a younger age, the numbers observed were closer to the published numbers: 14 ± 2 and 18 ± 2 GH146+ PNs in females and males, respectively (n = 12 ALs per group). The choice of the reporter used to reveal the postsynaptic signal is another factor that affects the numbers. In our attempts to optimize *trans*-Tango, we tested several available QUAS reporters as well as a few that we generated (data not shown). In the experiments aimed at revealing the totality of postsynaptic partners, we used the reporter that we generated as it yielded the best signal-to-noise ratio. However, the signal with this reporter was not sufficiently strong to obtain comprehensive labeling of postsynaptic partners in intersectional experiments where we used a conditional suppressor: we observed only 5 ± 2 and 8 ± 2 GH146+ PNs in females and males, respectively (n = 10 ALs per group). To avoid underrepresentation, we chose to use one of the more sensitive reporters (Potter et al., 2010) that consistently labeled more neurons even at the expense of potential false-positive signal. The use of this reporter could have contributed to the higher cell numbers observed in the intersectional experiments. In conclusion, *trans*-Tango is a powerful tool for generating hypotheses regarding connectivity. Like any other technique, connections revealed by *trans*-Tango will require further functional validation. Since *trans*-Tango provides genetic

access to the postsynaptic neurons, future versions of *trans*-Tango incorporating calcium indicators, such as GCaMP6 (Chen et al., 2013), as readout might facilitate such validation in circuits of interest.

When we assessed the age dependence of the *trans*-Tango signal, we observed three additional glomeruli in young animals when the ligand was driven in Or42b+ ORNs (Figure S4). By contrast, we never saw additional glomeruli when we analyzed Or67d+ ORNs (Figure S5). Careful examination of both the antennae and the AL revealed that these supernumerary glomeruli correspond to the neighboring neurons of Or42b+ ORNs within the ab1 sensilla (Or10a→DL1, Or92a→VA2, Gr21a→V), suggesting interactions between axons within the bundle. These interactions could be biologically significant or simply an artifact/noise of *trans*-Tango due to ligand mislocalization. Interestingly, when we drove ligand expression from Or92a+ ORNs that also reside in ab1 sensilla, we did not observe signal in the glomeruli of the other ORNs (Figure S6). Importantly, the strength of the *Or42b*-Gal4 and *Or92a*-Gal4 drivers is similarly high. Therefore, the different patterns of staining with these ORN populations likely reflect their biology.

In our validation experiments in the olfactory system, we induced ligand expression in different populations of ORNs and observed postsynaptic signal spanning the entire AL, as expected due to the panglomerular LNs (Chou et al., 2010). However, we noticed that the postsynaptic signal is not homogeneously distributed throughout the AL (Figures 2 and S2). Closer inspection revealed that the two classes of ORNs that detect pheromones (Or67d- and Or47b-expressing ORNs, targeting DA1 and VA1v, respectively) share the pattern of postsynaptic signal with sparser labeling of the medial aspect of the AL, an area that includes DM1 and VA2 (cognate glomeruli of Or42b and Or92a, respectively). By contrast, the two classes of ORNs known to detect food odors (Or42b and Or92a) share a different pattern of postsynaptic signal that is sparser in the lateral aspect of the AL, an area that includes DA1 and VA1v. The differences in postsynaptic patterns between the classes of glomeruli suggest that the segregation of food and pheromone channels observed in the targeting patterns of PNs in the LH (Jefferis et al., 2007) might be extended back to the AL, particularly to LNs. Such LNs that avoid certain glomeruli have been previously described (Chou et al., 2010). Interestingly, there is an inverse correlation between the odor-evoked firing rates of an LN and the number of glomeruli connected to it (Chou et al., 2010). It is conceivable that this inverse correlation is reflected in connectivity and extends to the numbers or sizes of synapses with ORNs. Therefore, it is possible that the connections between panglomerular LNs and ORNs are not strong enough to elicit robust *trans*-Tango signal. Notably, the synapses of panglomerular LNs were only revealed using a pre-synaptic marker (synaptotagmin-HA) and not by a post-synaptic marker (Chou et al., 2010). Therefore, it is conceivable that at least some of these LNs send output to all glomeruli while not receiving input from all glomeruli. Such LNs would not be detected by *trans*-Tango.

We revealed a connection between some glomeruli in the antennal lobe, including DA1 and VA1v, and the SEZ (Figures 1B, 2A, S2A, and Movie S1). These glomeruli are involved in pheromone detection, and the neuron connecting the two brain areas is Fru+ (Figure 3B and data not shown). Our observations could implicate this neuron in connecting olfactory pheromone responses and gustation. Other functional connections between pheromone detection and gustatory behavior have been recently reported (Clowney et al., 2015). The new features that we have identified in the well-studied olfactory circuits illustrate the power of *trans*-Tango to provide a comprehensive map of projections from a given neuron while maintaining the capacity to integrate clonal analysis for sparse labeling.

The implementation of *trans*-Tango in the gustatory system enabled us to identify previously unknown second-order neurons and trace their projections. Our study identified different areas in the protocerebrum (SMP, SIP and SLP) as the targets of the second-order neurons in the gustatory circuits. The SMP is associated with neuroendocrine centers, such as the pars intercerebralis (PI), which regulate various behaviors including feeding (Nässel et al., 2013). Several neuropeptides that control feeding behaviors are secreted from cells associated with the SMP (Nässel et al., 2013). For example, insulin-producing cells located in the PI have dendritic branches in the dorsal SMP (Kapan et al., 2012). Thus, the direct input from the SEZ to the SMP via the mSEZt (Figure 5, Movie S2) provides a possible pathway for integrating gustatory signals and the regulation of feeding behavior.

The SMP is also a target of the MB output neurons (MBONs) and it harbors the dendrites of dopaminergic neurons (DANs) that terminate in the MB (Aso et al., 2014). Similarly, the SIP and SLP contain processes of MBONs and DANs (Aso et al., 2014). In the MB, MBONs integrate dopamine input from DANs to mediate behavioral output. Several studies revealed that sugar-induced activity in a subset of DANs elicits appetitive memory (Burke et al., 2012; Liu et al., 2012). Remarkably, the projections through the three main gustatory tracts do not innervate the MB. This is in stark contrast to the olfactory circuits where second-order neurons massively project to the MB. Thus, gustatory information might be relayed into the MB at a higher level in the gustatory circuits. The direct input from the SEZ to the SMP, SIP, and SLP could provide the anatomical framework for gustatory learning. However, it is possible that such second-order gustatory neurons with termini in the MB do exist, but for some reason *trans*-Tango fails to reveal them.

The design of *trans*-Tango is modular, so it is not limited to tracing experiments. Since the readout of *trans*-Tango is transcription of a reporter gene, the system can be readily configured for functional experiments in which the activity of second-order neurons is altered (e.g., by incorporating optogenetic proteins as the reporter) or monitored (e.g., by incorporating calcium sensors as the reporter). Further, the *trans*-Tango design could be implemented in other organisms via viral delivery of the necessary components or by introducing them through genome editing techniques. In essence, *trans*-Tango provides genetic access to cells on the basis of their connectivity. Thus, *trans*-Tango expands the utility of molecular genetic techniques beyond the confines of a given cell. Finally, though we have presented *trans*-Tango as a neural circuit tracing technique, the same design could be used, with minor modifications, to study transient interactions between cells in other contexts, such as during development, in the immune system, or in cancer.

STAR★METHODS

Detailed methods are provided in the online version of this paper and include the following:

- KEY RESOURCES TABLE
- CONTACT FOR REAGENT AND RESOURCE SHARING
- EXPERIMENTAL MODEL AND SUBJECT DETAILS
  - Fly Strains
  - Generation of Transgenic Fly Lines
- METHOD DETAILS
  - Mosaic Analysis
  - Immunohistochemistry and Data Processing
- QUANTIFICATION AND STATISTICAL ANALYSIS
  - Quantification of Postsynaptic Neurons
  - Pixel Intensity Measurement

SUPPLEMENTAL INFORMATION

Supplemental Information includes ten figures, one table, and two movies and can be found with this article online at https://doi.org/10.1016/j.neuron.2017.10.011.

AUTHOR CONTRIBUTIONS

M.T., E.B.R., N.J.S., G.G.H., J.D.F., A.S., C.C.-F., M.J., J.R.S., and G.B. designed the experiments; M.T., E.B.R., N.J.S., G.G.H., J.D.F., A.S., C.C.-F., J.R.S., and N.N. performed the experiments; M.T., E.B.R., N.J.S., G.G.H., J.D.F., A.S., J.F.S., C.C.-F., and G.B. analyzed data; M.T., E.B.R., and G.B. wrote the manuscript. N.J.S., G.G.H., J.D.F., A.S., J.F.S., C.C.-F., M.J., and J.R.S. commented on the manuscript.

ACKNOWLEDGMENTS

This work was supported by NIH grants R21DCO14333, R01MH086920, R01MH105368, and R01DC013561 (G.B.), and by internal funds from Brown University: BIBS Innovation Award and OVPR Salomon and Seed Awards (G.B.). G.B. was supported in part by the Pew Charitable Trust. M.T. was supported by a fellowship from the Suna & İnan Kıraç Foundation and BIBS. E.B.R., G.G.H., and C.C.-F. were supported in part by a Karen T. Romer UTRA. N.J.S. was supported by grant number DGE1058262 from the National Science Foundation Graduate Research Fellowship Program. We thank Sasha Martinez-Machado for technical help. We thank Richard Axel, Liqun Luo, Alexander Fleischmann, Karla Kaun, Stavros Lomvardas, Mark Albers, and members of the Barnea lab for critical reading of the manuscript.

Received: September 13, 2016
Revised: June 30, 2017
Accepted: October 5, 2017
Published: October 26, 2017

REFERENCES

Aso, Y., Grübel, K., Busch, S., Friedrich, A.B., Siwanowicz, I., and Tanimoto, H. (2009). The mushroom body of adult Drosophila characterized by GAL4 drivers. J. Neurogenet. *23*, 156–172.

Aso, Y., Hattori, D., Yu, Y., Johnston, R.M., Iyer, N.A., Ngo, T.-T.B., Dionne, H., Abbott, L.F., Axel, R., Tanimoto, H., and Rubin, G.M. (2014). The neuronal architecture of the mushroom body provides a logic for associative learning. eLife *3*, e04577.

Barnea, G., Strapps, W., Herrada, G., Berman, Y., Ong, J., Kloss, B., Axel, R., and Lee, K.J. (2008). The genetic design of signaling cascades to record receptor activation. Proc. Natl. Acad. Sci. USA *105*, 64–69.

Bischof, J., Maeda, R.K., Hediger, M., Karch, F., and Basler, K. (2007). An optimized transgenesis system for Drosophila using germ-line-specific phiC31 integrases. Proc. Natl. Acad. Sci. USA *104*, 3312–3317.

Brand, A.H., and Perrimon, N. (1993). Targeted gene expression as a means of altering cell fates and generating dominant phenotypes. Development *118*, 401–415.

Briggman, K.L., and Bock, D.D. (2012). Volume electron microscopy for neuronal circuit reconstruction. Curr. Opin. Neurobiol. *22*, 154–161.

Burke, C.J., Huetteroth, W., Owald, D., Perisse, E., Krashes, M.J., Das, G., Gohl, D., Silies, M., Certel, S., and Waddell, S. (2012). Layered reward signalling through octopamine and dopamine in Drosophila. Nature *492*, 433–437.

Callaway, E.M., and Luo, L. (2015). Monosynaptic circuit tracing with glycoprotein-deleted rabies viruses. J. Neurosci. *35*, 8979–8985.

Chen, T.-W., Wardill, T.J., Sun, Y., Pulver, S.R., Renninger, S.L., Baohan, A., Schreiter, E.R., Kerr, R.A., Orger, M.B., Jayaraman, V., et al. (2013). Ultrasensitive fluorescent proteins for imaging neuronal activity. Nature *499*, 295–300.

Chen, Y., Akin, O., Nern, A., Tsui, C.Y.K., Pecot, M.Y., and Zipursky, S.L. (2014). Cell-type-specific labeling of synapses in vivo through synaptic tagging with recombination. Neuron *81*, 280–293.

Chiang, A.S., Lin, C.Y., Chuang, C.C., Chang, H.M., Hsieh, C.H., Yeh, C.W., Shih, C.T., Wu, J.J., Wang, G.T., Chen, Y.C., et al. (2011). Three-dimensional reconstruction of brain-wide wiring networks in Drosophila at single-cell resolution. Curr. Biol. *21*, 1–11.

Chou, T.-B., and Perrimon, N. (1992). Use of a yeast site-specific recombinase to produce female germline chimeras in Drosophila. Genetics *131*, 643–653.

Chou, Y.-H., Spletter, M.L., Yaksi, E., Leong, J.C.S., Wilson, R.I., and Luo, L. (2010). Diversity and wiring variability of olfactory local interneurons in the Drosophila antennal lobe. Nat. Neurosci. *13*, 439–449.

Clowney, E.J., Iguchi, S., Bussell, J.J., Scheer, E., and Ruta, V. (2015). Multimodal chemosensory circuits controlling male courtship in Drosophila. Neuron *87*, 1036–1049.

Clyne, P.J., Warr, C.G., and Carlson, J.R. (2000). Candidate taste receptors in Drosophila. Science *287*, 1830–1834.

Dahanukar, A., Lei, Y.T., Kwon, J.Y., and Carlson, J.R. (2007). Two Gr genes underlie sugar reception in Drosophila. Neuron *56*, 503–516.

Datta, S.R., Vasconcelos, M.L., Ruta, V., Luo, S., Wong, A., Demir, E., Flores, J., Balonze, K., Dickson, B.J., and Axel, R. (2008). The Drosophila pheromone cVA activates a sexually dimorphic neural circuit. Nature *452*, 473–477.

De Robertis, E.D.P., and Bennett, H.S. (1955). Some features of the submicroscopic morphology of synapses in frog and earthworm. J. Biophys. Biochem. Cytol. *1*, 47–58.

Dunipace, L., Meister, S., McNealy, C., and Amrein, H. (2001). Spatially restricted expression of candidate taste receptors in the Drosophila gustatory system. Curr. Biol. *11*, 822–835.

Fan, P., Manoli, D.S., Ahmed, O.M., Chen, Y., Agarwal, N., Kwong, S., Cai, A.G., Neitz, J., Renslo, A., Baker, B.S., and Shah, N.M. (2013). Genetic and neural mechanisms that inhibit Drosophila from mating with other species. Cell *154*, 89–102.

Feinberg, E.H., Vanhoven, M.K., Bendesky, A., Wang, G., Fetter, R.D., Shen, K., and Bargmann, C.I. (2008). GFP reconstitution across synaptic partners (GRASP) defines cell contacts and synapses in living nervous systems. Neuron *57*, 353–363.

Fishilevich, E., and Vosshall, L.B. (2005). Genetic and functional subdivision of the Drosophila antennal lobe. Curr. Biol. *15*, 1548–1553.

Fishilevich, E., Domingos, A.I., Asahina, K., Naef, F., Vosshall, L.B., and Louis, M. (2005). Chemotaxis behavior mediated by single larval olfactory neurons in Drosophila. Curr. Biol. *15*, 2086–2096.

Fortin, J.-P., Zhu, Y., Choi, C., Beinborn, M., Nitabach, M.N., and Kopin, A.S. (2009). Membrane-tethered ligands are effective probes for exploring class B1 G protein-coupled receptor function. Proc. Natl. Acad. Sci. USA *106*, 8049–8054.

Gibson, D.G., Young, L., Chuang, R.Y., Venter, J.C., Hutchison, C.A., 3rd, and Smith, H.O. (2009). Enzymatic assembly of DNA molecules up to several hundred kilobases. Nat. Methods *6*, 343–345.

Gordon, M.D., and Scott, K. (2009). Motor control in a Drosophila taste circuit. Neuron *61*, 373–384.

Grabe, V., Baschwitz, A., Dweck, H.K.M., Lavista-Llanos, S., Hansson, B.S., and Sachse, S. (2016). Elucidating the neuronal architecture of olfactory glomeruli in the Drosophila antennal lobe. Cell Rep. *16*, 3401–3413.

Groth, A.C., Fish, M., Nusse, R., and Calos, M.P. (2004). Construction of transgenic Drosophila by using the site-specific integrase from phage phiC31. Genetics *166*, 1775–1782.

Harris, D.T., Kallman, B.R., Mullaney, B.C., and Scott, K. (2015). Representations of taste modality in the Drosophila brain. Neuron *86*, 1449–1460.

Hong, S.-T., Bang, S., Paik, D., Kang, J., Hwang, S., Jeon, K., Chun, B., Hyun, S., Lee, Y., and Kim, J. (2006). Histamine and its receptors modulate temperature-preference behaviors in Drosophila. J. Neurosci. *26*, 7245–7256.

Hong, W., Zhu, H., Potter, C.J., Barsh, G., Kurusu, M., Zinn, K., and Luo, L. (2009). Leucine-rich repeat transmembrane proteins instruct discrete dendrite targeting in an olfactory map. Nat. Neurosci. *12*, 1542–1550.

Huh, Y., Oh, M.S., Leblanc, P., and Kim, K.-S. (2010). Gene transfer in the nervous system and implications for transsynaptic neuronal tracing. Expert Opin. Biol. Ther. *10*, 763–772.

Inagaki, H.K., Ben-Tabou de-Leon, S., Wong, A.M., Jagadish, S., Ishimoto, H., Barnea, G., Kitamoto, T., Axel, R., and Anderson, D.J. (2012). Visualizing neuromodulation in vivo: TANGO-mapping of dopamine signaling reveals appetite control of sugar sensing. Cell *148*, 583–595.

Ito, K., Shinomiya, K., Ito, M., Armstrong, J.D., Boyan, G., Hartenstein, V., Harzsch, S., Heisenberg, M., Homberg, U., Jenett, A., et al.; Insect Brain Name Working Group (2014). A systematic nomenclature for the insect brain. Neuron *81*, 755–765.

Jagadish, S., Barnea, G., Clandinin, T.R., and Axel, R. (2014). Identifying functional connections of the inner photoreceptors in Drosophila using Tango-Trace. Neuron *83*, 630–644.

Jefferis, G.S.X.E., Potter, C.J., Chan, A.M., Marin, E.C., Rohlfing, T., Maurer, C.R., Jr., and Luo, L. (2007). Comprehensive maps of Drosophila higher olfactory centers: spatially segregated fruit and pheromone representation. Cell *128*, 1187–1203.

Kain, P., and Dahanukar, A. (2015). Secondary taste neurons that convey sweet taste and starvation in the Drosophila brain. Neuron *85*, 819–832.

Kapan, N., Lushchak, O.V., Luo, J., and Nässel, D.R. (2012). Identified peptidergic neurons in the Drosophila brain regulate insulin-producing cells, stress responses and metabolism by coexpressed short neuropeptide F and corazonin. Cell. Mol. Life Sci. *69*, 4051–4066.

Kim, H., Kirkhart, C., and Scott, K. (2017). Long-range projection neurons in the taste circuit of Drosophila. eLife *6*, 1–24.

Kimura, K., Ote, M., Tazawa, T., and Yamamoto, D. (2005). Fruitless specifies sexually dimorphic neural circuitry in the Drosophila brain. Nature *438*, 229–233.

Kreher, S.A., Kwon, J.Y., and Carlson, J.R. (2005). The molecular basis of odor coding in the Drosophila larva. Neuron *46*, 445–456.

Krstenansky, J.L., Trivedi, D., Johnson, D., and Hruby, V.J. (1986). Conformational considerations in the design of a glucagon analog with increased receptor binding and adenylate cyclase potencies. J. Am. Chem. Soc. *108*, 1696–1698.

Kurtovic, A., Widmer, A., and Dickson, B.J. (2007). A single class of olfactory neurons mediates behavioural responses to a Drosophila sex pheromone. Nature *446*, 542–546.

Kwon, J.Y., Dahanukar, A., Weiss, L.A., and Carlson, J.R. (2014). A map of taste neuron projections in the Drosophila CNS. J. Biosci. *39*, 565–574.

Lee, T., and Luo, L. (1999). Mosaic analysis with a repressible cell marker for studies of gene function in neuronal morphogenesis. Neuron *22*, 451–461.

Liu, C., Plaçais, P.-Y., Yamagata, N., Pfeiffer, B.D., Aso, Y., Friedrich, A.B., Siwanowicz, I., Rubin, G.M., Preat, T., and Tanimoto, H. (2012). A subset of dopamine neurons signals reward for odour memory in Drosophila. Nature *488*, 512–516.

Lo, L., and Anderson, D.J. (2011). A Cre-dependent, anterograde transsynaptic viral tracer for mapping output pathways of genetically marked neurons. Neuron *72*, 938–950.

Macpherson, L.J., Zaharieva, E.E., Kearney, P.J., Alpert, M.H., Lin, T.-Y., Turan, Z., Lee, C.-H., and Gallio, M. (2015). Dynamic labelling of neural connections in multiple colours by trans-synaptic fluorescence complementation. Nat. Commun. *6*, 10024.

Markstein, M., Pitsouli, C., Villalta, C., Celniker, S.E., and Perrimon, N. (2008). Exploiting position effects and the gypsy retrovirus insulator to engineer precisely expressed transgenes. Nat. Genet. *40*, 476–483.

Miyazaki, T., Lin, T.-Y., Ito, K., Lee, C.-H., and Stopfer, M. (2015). A gustatory second-order neuron that connects sucrose-sensitive primary neurons and a distinct region of the gnathal ganglion in the Drosophila brain. J. Neurogenet. *29*, 144–155.

Morante, J., and Desplan, C. (2008). The color-vision circuit in the medulla of Drosophila. Curr. Biol. *18*, 553–565.

Nässel, D.R. (1999). Histamine in the brain of insects: a review. Microsc. Res. Tech. *44*, 121–136.

Nässel, D.R., Kubrak, O.I., Liu, Y., Luo, J., and Lushchak, O.V. (2013). Factors that regulate insulin producing cells and their output in Drosophila. Front. Physiol. *4*, 252.

Nern, A., Pfeiffer, B.D., and Rubin, G.M. (2015). Optimized tools for multicolor stochastic labeling reveal diverse stereotyped cell arrangements in the fly visual system. Proc. Natl. Acad. Sci. USA *112*, E2967–E2976.

Nicolaï, L.J.J., Ramaekers, A., Raemaekers, T., Drozdzecki, A., Mauss, A.S., Yan, J., Landgraf, M., Annaert, W., and Hassan, B.A. (2010). Genetically encoded dendritic marker sheds light on neuronal connectivity in Drosophila. Proc. Natl. Acad. Sci. USA *107*, 20553–20558.

Patterson, G.H., and Lippincott-Schwartz, J. (2002). A photoactivatable GFP for selective photolabeling of proteins and cells. Science *297*, 1873–1877.

Pfeiffer, B.D., Jenett, A., Hammonds, A.S., Ngo, T.-T.B., Misra, S., Murphy, C., Scully, A., Carlson, J.W., Wan, K.H., Laverty, T.R., et al. (2008). Tools for neuroanatomy and neurogenetics in Drosophila. Proc. Natl. Acad. Sci. USA *105*, 9715–9720.

Pfeiffer, B.D., Ngo, T.T.-T.B., Hibbard, K.L., Murphy, C., Jenett, A., Truman, J.W., and Rubin, G.M. (2010). Refinement of tools for targeted gene expression in Drosophila. Genetics *186*, 735–755.

Pfeiffer, B.D., Truman, J.W., and Rubin, G.M. (2012). Using translational enhancers to increase transgene expression in Drosophila. Proc. Natl. Acad. Sci. USA *109*, 6626–6631.

Potter, C.J., and Luo, L. (2011). Using the Q system in Drosophila melanogaster. Nat. Protoc. *6*, 1105–1120.

Potter, C.J., Tasic, B., Russler, E.V., Liang, L., and Luo, L. (2010). The Q system: a repressible binary system for transgene expression, lineage tracing, and mosaic analysis. Cell *141*, 536–548.

Ramaekers, A., Magnenat, E., Marin, E.C., Gendre, N., Jefferis, G.S.X.E., Luo, L., and Stocker, R.F. (2005). Glomerular maps without cellular redundancy at successive levels of the Drosophila larval olfactory circuit. Curr. Biol. *15*, 982–992.

Ramón y Cajal, S. (1888). No Estructura de los centros nerviosos de las aves. Rev. Trim. Histol. Norm. Pat *1*, 1–10.

Root, C.M., Ko, K.I., Jafari, A., and Wang, J.W. (2011). Presynaptic facilitation by neuropeptide signaling mediates odor-driven food search. Cell *145*, 133–144.

Ruta, V., Datta, S.R., Vasconcelos, M.L., Freeland, J., Looger, L.L., and Axel, R. (2010). A dimorphic pheromone circuit in Drosophila from sensory input to descending output. Nature *468*, 686–690.

Scott, K., Brady, R., Jr., Cravchik, A., Morozov, P., Rzhetsky, A., Zuker, C., and Axel, R. (2001). A chemosensory gene family encoding candidate gustatory and olfactory receptors in Drosophila. Cell *104*, 661–673.

Seki, Y., Rybak, J., Wicher, D., Sachse, S., and Hansson, B.S. (2010). Physiological and morphological characterization of local interneurons in the Drosophila antennal lobe. J. Neurophysiol. *104*, 1007–1019.

Semmelhack, J.L., and Wang, J.W. (2009). Select Drosophila glomeruli mediate innate olfactory attraction and aversion. Nature *459*, 218–223.

Sherrington, C.S. (1906). Observations on the scratch-reflex in the spinal dog. J. Physiol. *34*, 1–50.

Strutz, A., Soelter, J., Baschwitz, A., Farhan, A., Grabe, V., Rybak, J., Knaden, M., Schmuker, M., Hansson, B.S., and Sachse, S. (2014). Decoding odor quality and intensity in the Drosophila brain. eLife *3*, e04147.

Thoma, V., Knapek, S., Arai, S., Hartl, M., Kohsaka, H., Sirigrivatanawong, P., Abe, A., Hashimoto, K., and Tanimoto, H. (2016). Functional dissociation in sweet taste receptor neurons between and within taste organs of Drosophila. Nat. Commun. *7*, 10678.

Vosshall, L.B., and Stocker, R.F. (2007). Molecular architecture of smell and taste in Drosophila. Annu. Rev. Neurosci. *30*, 505–533.

Wang, Z., Singhvi, A., Kong, P., and Scott, K. (2004). Taste representations in the Drosophila brain. Cell *117*, 981–991.

Wilder, E.L., and Perrimon, N. (1995). Dual functions of wingless in the Drosophila leg imaginal disc. Development *121*, 477–488.

Wu, J.S., and Luo, L. (2006). A protocol for dissecting Drosophila melanogaster brains for live imaging or immunostaining. Nat. Protoc. *1*, 2110–2115.

Yapici, N., Cohn, R., Schusterreiter, C., Ruta, V., and Vosshall, L.B. (2016). A Taste Circuit that Regulates Ingestion by Integrating Food and Hunger Signals. Cell *165*, 715–729.

Yu, J.Y., Kanai, M.I., Demir, E., Jefferis, G.S.X.E., and Dickson, B.J. (2010). Cellular organization of the neural circuit that drives Drosophila courtship behavior. Curr. Biol. *20*, 1602–1614.

Zhang, Y.Q., Rodesch, C.K., and Broadie, K. (2002). Living synaptic vesicle marker: synaptotagmin-GFP. Genesis *34*, 142–145.

Zingg, B., Chou, X.L., Zhang, Z.G., Mesik, L., Liang, F., Tao, H.W., and Zhang, L.I. (2017). AAV-mediated anterograde transsynaptic tagging: mapping corticocollicular input-defined neural pathways for defense behaviors. Neuron *93*, 33–47.

STAR★METHODS

KEY RESOURCES TABLE

REAGENT or RESOURCE	SOURCE	IDENTIFIER
Antibodies		
anti-GFP (rabbit polyclonal)	Thermo Fisher Scientific	Cat# A11122; RRID: AB_221569
anti-HA (mouse monoclonal)	Covance	Cat# MMS-101P; clone# HA.11; RRID: AB_2314672
anti-HA (rat monoclonal)	Roche	Cat# 11867423001; clone# 3F10; RRID: AB_390918
anti-myc (mouse monoclonal)	Covance	Cat# MMS-150P; clone# 9E10; RRID: AB_291322
anti-Brp (mouse monoclonal)	DSHB	Cat# nc82; RRID: AB_2314866
anti-Ncad (rat monoclonal)	DSHB	Cat# DN-Ex 8; RRID: AB_528121
Donkey anti-rabbit IgG (H+L) Alexa Fluor 488	Thermo Fisher Scientific	Cat# A-21206; RRID: AB_2535792
Donkey anti-mouse IgG (H+L) Alexa Fluor 555	Thermo Fisher Scientific	Cat# A-31570; RRID: AB_2536180
Donkey anti-mouse IgG (H+L) Alexa Fluor 647	Thermo Fisher Scientific	Cat# A-31571; RRID: AB_162542
Goat anti-rat IgG (H+L) Alexa Fluor 555	Thermo Fisher Scientific	Cat# A-21434; RRID: AB_2535855
Goat anti-rat IgG (H+L) Alexa Fluor 647	Thermo Fisher Scientific	Cat# A-21247; RRID: AB_141778
Bacterial and Virus Strains		
MAX Efficiency DH5α Competent Cells	Thermo Fisher Scientific	Cat# 18258012
NEB Stable Competent *E. coli* (High Efficiency)	NEB	Cat# C3040H
SURE 2 Supercompetent Cells	Agilent	Cat# 200152
Experimental Models: Organisms/Strains		
Drosophila: Or42a-Gal4	Bloomington Drosophila Stock Center	RRID: BDSC_9969
Drosophila: Or42b-Gal4	Bloomington Drosophila Stock Center	RRID: BDSC_9971
Drosophila: Or47b-Gal4	Bloomington Drosophila Stock Center	RRID: BDSC_9983
Drosophila: Or92a-Gal4	Bloomington Drosophila Stock Center	RRID: BDSC_23140
Drosophila: Or67d^{Gal4}	B. Dickson, Kurtovic et al., 2007	FlyBase: FBti0168583
Drosophila: Orco-Gal4	Bloomington Drosophila Stock Center	RRID: BDSC_23292
Drosophila: Gr64f-Gal4	Bloomington Drosophila Stock Center	RRID: BDSC_57669
Drosophila: lGMR-Gal4	Bloomington Drosophila Stock Center	RRID: BDSC_8121
Drosophila: MB247-Gal4	Bloomington Drosophila Stock Center	RRID: BDSC_50742
Drosophila: FRT^{G13}	Bloomington Drosophila Stock Center	RRID: BDSC_1956
Drosophila: FRT^{G13}, tubP-QS(5A)	Bloomington Drosophila Stock Center	RRID: BDSC_30133
Drosophila: hsFLP	Bloomington Drosophila Stock Center	RRID: BDSC_7
Drosophila: hsFLP	Bloomington Drosophila Stock Center	RRID: BDSC_1813
Drosophila: GH146-FLP	L. Luo, Hong et al., 2009	FlyBase: FBtp0053491
Drosophila: fru^{FLP}	B. Dickson, Yu et al., 2010	FlyBase: FBti0168739
Drosophila: UAS-syt::GFP	Bloomington Drosophila Stock Center	RRID: BDSC_6924
Drosophila; UAS-syt::GFP, UAS-DenMark	Bloomington Drosophila Stock Center	RRID: BDSC_33065
Drosophila: UAS-mtdTomato	Bloomington Drosophila Stock Center	RRID: BDSC_32221
Drosophila: QUAS-FRT-STOP-FRT-mCD8::GFP	Bloomington Drosophila Stock Center	RRID: BDSC_30136
Drosophila: hsFLP, UAS-mCD8::GFP, QUAS-mtdTomato(3xHA)	Bloomington Drosophila Stock Center	RRID: BDSC_30118
Drosophila: UAS-myrGFP, QUAS-mtdTomato(3xHA)	This study	N/A
Drosophila: tubP-FRT-QS-FRT	This study	N/A
Drosophila: trans-Tango	This study	N/A

(*Continued on next page*)

Continued

REAGENT or RESOURCE	SOURCE	IDENTIFIER
Recombinant DNA		
human ICAM1	R&D Systems, VersaClone	Cat# RDC1030
pattB-QF-hsp70	Potter et al., 2010	Addgene Cat# 24368
pBluescript KS+ (pBS KS+)	Agilent	Cat# 212207
pJET1.2	Thermo Fisher Scientific	Cat# K1231
pJFRC12	Pfeiffer et al., 2010	Addgene Cat# 26222
pJFRC81	Pfeiffer et al., 2012	Addgene Cat# 36432
pQUAST-mtdT-3xHA	Potter et al., 2010	Addgene Cat# 24354
ptubP-QS	Potter et al., 2010	Addgene Cat# 24352
pUASTattB	Bischof et al., 2007	FlyBase: FBmc0003002
tubP-FRT>Gal80-6-FRT >	Nern et al., 2015	Addgene Cat# 63173
trans-Tango	This study	N/A
UAS-myrGFP, QUAS-mtdTomato(3xHA)	This study	N/A
tubP-FRT-QS-FRT	This study	N/A
Software and Algorithms		
Adobe Photoshop CC	Adobe	RRID: SCR_014199
Adobe Illustrator CC	Adobe	RRID: SCR_010279
ZEN	Carl Zeiss Microscopy	Version 2.1 (blue edition)
Fiji	http://fiji.sc	RRID: SCR_002285
Imaris	Bitplane AG	Version 8.4.1; RRID: SCR_007370

CONTACT FOR REAGENT AND RESOURCE SHARING

Further information and requests for resources and reagents should be directed to and will be fulfilled by the Lead Contact, Gilad Barnea (gilad_barnea@brown.edu).

EXPERIMENTAL MODEL AND SUBJECT DETAILS

Fly Strains

All fly lines used in this study were maintained at either 18°C or 21°C on standard cornmeal-agar-molasses media. Unless otherwise stated, crosses and the resulting progeny that were analyzed for this study were maintained at 18°C in humidity-controlled chambers under 12-hr light/dark cycles. The fly lines used in this study are as follows: *Or42a*-Gal4 (BDSC#9969), *Or42b*-Gal4 (BDSC#9971), *Or47b*-Gal4 (BDSC#9983), *Or92a*-Gal4 (BDSC#23140) (Fishilevich and Vosshall, 2005); $Or67d^{Gal4}$ (Kurtovic et al., 2007); *Orco*-Gal4 (*Or83b*-Gal4; BDSC#23292) (Kreher et al., 2005); *Gr64f*-Gal4 (BDSC#57669) (Dahanukar et al., 2007); *IGMR*-Gal4 (BDSC#8121); *MB247*-Gal4 (BDSC#50742) (Aso et al., 2009); FRT^{G13} (BDSC#1956) (Wilder and Perrimon, 1995); FRT^{G13}, *tubP*-QS(5A) (BDSC#30133) (Potter et al., 2010); hsFLP (BDSC#7), hsFLP (BDSC#1813) (Chou and Perrimon, 1992); *GH146*-$FLP^{3xP3\text{-}DsRED}$ (Hong et al., 2009); fru^{FLP} (Yu et al., 2010); *UAS*-syt::GFP (BDSC#6924) (Zhang et al., 2002); *UAS*-syt::GFP, *UAS*-DenMark (BDSC#33065) (Nicolaï et al., 2010); *QUAS-FRT-STOP-FRT*-mCD8::GFP (BDSC#30136), hsFLP, *UAS*-mCD8::GFP, *QUAS*-mtdTomato(3xHA) (BDSC#30118) (Potter et al., 2010); *UAS*-mtdTomato (BDSC#32221) (Pfeiffer et al., 2010); *UAS*-myrGFP, *QUAS*-mtdTomato(3xHA); *tubP-FRT-QS-FRT* and *trans*-Tango (described below). A list of the full genotypes for the flies used in each figure is in Table S1.

Generation of Transgenic Fly Lines

Plasmids used in this study to generate transgenic fly lines (described in Figure S1A in detail) were constructed using standard cloning techniques including restriction digest and ligation, PCR assembly and Gibson Assembly, and were sequenced before injection. The plasmid used for the generation of *trans*-Tango transgenic flies was constructed by standard molecular cloning techniques. A scaffold of unique restriction sites was ligated into pBluescript KS+ (pBS KS+; Agilent). The following DNA sequences were PCR amplified to add appropriate restriction sites and ligated into the pJET1.2 vector (Thermo Fisher Scientific): the Elav promoter, obtained from *Drosophila* genomic DNA; the Arrestin::TEV protease fusion (hArr::TEV) (Barnea et al., 2008); the SV40 polyadenylation sequence (SV40pA), which was obtained from pUASTattB vector (Bischof et al., 2007); the nSyb promoter; the *Drosophila* Synthetic Core Promoter (DSCP) (Pfeiffer et al., 2008); human glucagon receptor; the serine TEV cleavage site (TEVcs); QF, obtained from

pattB-QF-hsp70 (Addgene, 24368) (Potter et al., 2010), and the hsp70 polyadenylation sequence (hsp70pA), obtained from pattB-QF-hsp70. These sequences were digested from pJET1.2 and ligated into the pBS KS+ scaffold in a hierarchical manner, resulting in two cassettes from 5′ to 3′: Elav-hArr::TEV-SV40pA, nSyb-DSCP-hGCGR::TEVcs::QF-hsp70pA (panneuronal cassettes). A second scaffold of unique restriction sites was generated and ligated into pUASTattB between the white gene and the attB sequence. The panneuronal cassettes were digested and ligated in an inverted manner (3′ to 5′) into the modified pUASTattB scaffold. To assemble the *trans*-Tango ligand, the following DNA sequences were amplified with overlapping 5′ and 3′ sequences: 10xUAS-IVS-Syn21, obtained from pJFRC81 (Addgene, 36432) (Pfeiffer et al., 2012); trypsin signal peptide, followed by human glucagon peptide, six Glycine-Asparagine (GN) repeats, myc-tag, and nine GN repeats (Fortin et al., 2009); the extracellular domain of human ICAM1, from the last isoleucine residue of the transmembrane domain to the N terminus of the extracellular domain, obtained from cDNA (VersaClone); *Drosophila* Neurexin1, from the C-terminal cytosolic tail through the transmembrane domain (not including the last isoleucine residue), obtained from *Drosophila* genomic DNA, and the p10 polyadenylation sequence, obtained from pJFRC81. These sequences were covalently fused to each other by Gibson Assembly (New England Biolabs) (Gibson et al., 2009). They were subsequently amplified in two pieces to introduce super-agonist mutations to the glucagon peptide (Krstenansky et al., 1986), and were finally assembled by Gibson Assembly, from 5′ to 3′, into the pUASTattB scaffold containing the panneuronal cassettes in the opposite orientation.

The plasmid used for the generation of reporter flies, *UAS*-myrGFP and *QUAS*-mtdTomato(3xHA), was constructed by Gibson Assembly. The *5xQUAS*-mtdTomato(3xHA) sequence, obtained from *pQUAST*-mtdT-3xHA (Addgene, 24354) (Potter et al., 2010), and the hsp70pA sequence were amplified by PCR with appropriate overlaps. These sequences were assembled into the pJFRC12 plasmid (Addgene, 26222) (Pfeiffer et al., 2010) following the existing GFP cassette and in the reverse orientation.

The plasmid used to generate *tubP-FRT-QS-FRT* conditional suppressor transgenic flies was constructed by Gibson Assembly. The tubulin promoter and the first FRT site, as well as the WPRE, the SV40pA and the second FRT site were amplified from *tubP-FRT>GAL80-6-FRT>* (Addgene, 63173) (Nern et al., 2015), and the QS sequence was amplified from *ptubP*-QS (Addgene, 24352) (Potter et al., 2010). All PCR amplifications were performed with the appropriate overlaps and the pieces were assembled into the pUASTattB vector.

Lines of transgenic flies were generated by site-directed genomic integration of constructs using the PhiC31 system (Groth et al., 2004; Markstein et al., 2008). The *trans*-Tango construct containing ligand, synthetic receptor and hArr::TEV genes was incorporated at the attP40 site. The construct containing the reporter genes, *UAS*-myrGFP and *QUAS*-mtdTomato(3xHA), was incorporated at the su(Hw)attP8 site. The conditional suppressor construct, *tubP-FRT-QS-FRT*, was incorporated at the VK00018 site.

METHOD DETAILS

Mosaic Analysis

MARCM experiments for postsynaptic signal in the olfactory and gustatory systems were performed as described previously (Lee and Luo, 1999; Potter and Luo, 2011). Briefly, flies of genotype *UAS-myrGFP, QUAS-mtdTomato(3xHA), hsFLP (X); trans-Tango, FRT^{G13}, tubP-QS(5A)/FRT^{G13} (II); Or67d-Gal4/+ (III)*, and *UAS-myrGFP, QUAS-mtdTomato(3xHA), hsFLP (X); trans-Tango, FRT^{G13}, tubP-QS(5A)/FRT^{G13}, Gr64f-Gal4 (II)* were raised at 18°C and transiently heat-shocked in a 37°C water bath for 2 min to 1 hr during early third instar larval stage.

Intersectional analysis of postsynaptic signal of Or67d+ neurons was performed using flies of the following genotypes: *w (X); trans-Tango, GH146-FLP/+ (II); Or67d-Gal4/QUAS-FRT-STOP-FRT-mCD8::GFP, UAS-mtdTomato (III),* and *w (X); trans-Tango/+ (II); Or67d-Gal4, fru-FLP/QUAS-FRT-STOP-FRT-mCD8::GFP, UAS-mtdTomato (III)*.

Intersectional FLP-out analysis of postsynaptic signal of Or42a+ neurons was performed using larvae of the following genotypes: *UAS-myrGFP, QUAS-mtdTomato(3xHA) (X); trans-Tango, GH146-FLP, tubP-FRT-QS-FRT/Or42a-Gal4 (II)*.

Clonal FLP-out analysis of postsynaptic signal of Gr64f+ neurons was performed using flies of the following genotypes: *UAS-myrGFP, QUAS-mtdTomato(3xHA) (X); trans-Tango, tubP-FRT-QS-FRT/Gr64f-Gal4, hsFLP (II)*. Flies were raised at 18°C and transiently heat-shocked in a 37°C water bath for 5 to 15 min during late pupal stages to generate random clones that lack QS expression.

Immunohistochemistry and Data Processing

Immunohistochemistry experiments were performed as described previously (Wu and Luo, 2006) with minor modifications. Briefly, either adult flies that are 15-20 days old (unless otherwise noted) or third instar wandering larvae were cold anaesthetized on ice and dissected in PBS or 0.03%PBST (T stands for Triton X-100; Fisher Bioreagents, BP151-500). After a 30 min fixation of samples in 4% PFA/0.3%PBST at room temperature (RT) or an overnight fixation in 2%PFA/0.3%PBST at 4°C, samples were washed four times for 15 min in 0.3%PBST at RT, blocked in 5% heat-inactivated donkey or equine serum (diluted from 100% with 0.3% PBST) for 30 min at RT, and incubated with primary antibodies for two overnights at 4°C. Samples were washed again four times for 15 min at RT and incubated with secondary antibodies for two overnights at 4°C. The samples were then washed again four times for 15 min at RT and mounted on a slide (Fisherbrand Superfrost Plus, 12-550-15) using Fluoromount-G mounting medium (SouthernBiotech, 0100-01). Samples used for generating supplemental videos and cell-counting data were cleared as described previously (Nern et al., 2015). The primary and secondary antibodies were diluted in blocking solution. The primary antibodies used in this study were anti-GFP rabbit (Thermo Fisher Scientific, A11122; 1:1,000), anti-HA mouse (Covance, MMS-101P; 1:250), anti-HA rat (Roche,

11867423001; 1:100), anti-myc mouse (Covance, MMS-150P; 1:250), anti-Brp mouse (nc82; DSHB; 1:50) and anti-Ncad rat (DSHB; 1:20). Secondary antibodies were diluted at 1:1,000 and were as follows: donkey anti-rabbit Alexa Fluor 488, donkey anti-mouse Alexa Fluor 555, goat anti-rat Alexa Fluor 555, donkey anti-mouse Alexa Fluor 647 and goat anti-rat Alexa Fluor 647. Images were taken using confocal microscopy (Zeiss, LSM800) with ZEN software (Zeiss, version 2.1) with auto Z brightness correction to generate a homogeneous signal where it seemed necessary, and were formatted using Fiji software (http://fiji.sc) or Adobe Photoshop CC. Supplemental videos were generated using Imaris software (Bitplane AG, version 8.4.1) with tiled confocal images taken with low laser settings. Figures were generated using Adobe Illustrator CC.

QUANTIFICATION AND STATISTICAL ANALYSIS

Quantification of Postsynaptic Neurons

Confocal images taken with laser and microscope settings held constant within groups were used to quantify the postsynaptic neurons revealed by *trans*-Tango. Cell bodies were counted manually using cell counter plugin in Fiji in a non-stringent manner: cells were counted even if the signal in them was weak in order to reveal any potential connection. Number of samples used for cell-counting data is reported in the results and discussion sections.

Pixel Intensity Measurement

HA and myc immunofluorescence were imaged in separate channels using confocal microscopy, and all laser and microscope settings were held constant for all brains. Pixel intensities were calculated using Fiji. For a given z stack of a brain, the selection brush feature was used to draw a circular ROI of fixed diameter over either the entire left antennal lobe (to quantify HA staining) or the entire left DA1 glomerulus (to quantify myc staining). For each frame of the stack, average pixel intensity within the ROI was calculated. For myc, this average pixel intensity in each frame was normalized by subtracting out the average pixel intensity of an unstained region within the antennal lobe. The maximum value of this average pixel intensity across all frames of the stack was determined and reported. Number of samples used to determine the average pixel intensity is reported in the figure legend.